Computational and Experimental Investigations of Defect Interaction and Ionic Conductivity in Doped Zirconia

Qiannan Xue,[1] Xiaowei Huang,[1,2] Ligen Wang,[3,*] He Zhang,[1,2] and Jianxing Zhang[1]

[1]*National Engineering Research Center for Rare Earth Materials, General Research Institute for Nonferrous Metals, Beijing 100088, China*
[2]*Griam Advanced Materials Co., Ltd., Beijing 100088, China*
[3]*State Key Laboratory of Nonferrous Metals and Processes, General Research Institute for Nonferrous Metals, Beijing 100088, China*

Zirconia is a promising electrolyte material that has been widely used in solid-oxide fuel cells. In this paper, the effects of defect interaction on the ionic conductivity of scandia- and yttria-doped zirconia are systematically investigated by density-functional-theory calculations and experimental verification. We theoretically predict the doping concentrations of the tetragonal-to-cubic phase transition to be 18 at. % for Sc^{3+} and 9 at. % for Y^{3+}, which are in reasonable agreement with the experimental values. Oxygen-vacancy-formation energies, oxygen-vacancy-dopant binding energies, and diffusion barriers are calculated to evaluate ionic conduction properties. Our calculated results show that the binding-energy variances of different defect configurations in scandia-doped zirconia are markedly lower than those in yttria-doped zirconia. Diffusion barriers are calculated using the saddle-point method, and the corresponding experiments are carried out to verify the diffusion-barrier results.

I. INTRODUCTION

Solid-oxide fuel cells (SOFCs) are one of the most promising technologies to cope with a future energy crisis because they are environmentally friendly and highly efficiency [1]. However, the key problem that hinders SOFC commercialization is the low conductivity of solid electrolytes at low operating temperatures [2]. The conductivity decay problem after long-term usage is another serious constraint. Therefore, it is crucial to improve the conductivity and stability of zirconia-based electrolytes to meet the demand of lower-temperature operations [3].

Zirconia has three morphologies. The monoclinic (*m*) phase is a low-temperature phase, which transforms to the tetragonal (*t*) phase and cubic (*c*) phase at 1170 and 2370 °C, respectively. Cubic zirconia is stable up to its melting point of 2680 °C [4]. The phase transformations are accompanied by a large volume change (~7%) [5], which causes the material to crack under thermal cycling. As a result, zirconia must be stabilized to a specific phase structure. The *c* phase shows the highest conductivity because of its high structural symmetry. It consists of a Zr-cation fcc lattice and an oxygen-anion simple cubic lattice. Oxygen ions occupy the tetrahedral interstices while all the octahedral interstices are empty. This offers some open

paths for oxygen ions to diffuse. Therefore, the *c* phase is desired for obtaining a high ionic conductivity [6].

The *c* phase can be stabilized to room temperature by doping aliovalent elements, such as Sc, Y, Bi, Yb, and Mg. These aliovalent dopants can cause some oxygen vacancies in the doped zirconia [7]. One of the most commonly used electrolytes for SOFCs at high temperature (~1000 °C) is 8 at. % Y_2O_3-ZrO_2 (8YSZ) [8]. However, the high operation temperature causes many serious problems, such as the high cost of SOFC interconnects, active reactions between anodes and electrolytes, degradation of electrodes, etc. Therefore, many experimental and theoretical efforts are devoted to reducing the operation temperature of SOFCs [9]. In this respect, scandia-doped zirconia (ScSZ) attracts considerable attention because it is known to have the highest conductivity among all zirconia-based electrolytes at intermediate operating temperatures (650–850 °C). Conductivity of 10 at. % Sc_2O_3-ZrO_2 (10ScSZ) is reported to be 230 mS/cm at 900 °C compared to 110 mS/cm for 8YSZ under the same test conditions [1]. As a result, 10ScSZ offers a potential way to develop intermediate-temperature solid-oxide fuel cells (IT SOFCs).

To calculate the energetic and electronic structures of solids, the density-functional-theory (DFT) method has proven to be one of the most accurate. Many first-principles calculations have been performed to reveal

ionic conduction mechanisms from the atomic levels. The phase structures, defect ordering, and vacancy behaviors of doped zirconia are widely studied [10–16]. For example, the phase-transition doping concentrations were predicted in our previous paper [16]. The defect ordering in YSZ is studied using the molecular dynamics simulation method [10]. Stafford investigated the ionic conductivity of doped ZrO_2 and found that the vacancy binding energy increases with an increase of dopant cation radii [17]. Miller and his team found that oxygen vacancies occupy the neighboring anion sites, which causes age-related degradation over time [14]. However, the influences of doping and defect interactions on the ionic conductivity in zirconia-based electrolytes are not yet thoroughly understood.

In this paper, Y_2O_3 and Sc_2O_3 were chosen as representative dopants to clarify the inner influences of dopants on ionic conduction properties by DFT calculations. Total energies (E_{tot}) for various doping concentrations were calculated to predict the phase-transition points. Oxygen-vacancy-formation energies, oxygen-vacancy-dopant binding energies, and diffusion barriers are calculated to evaluate the ionic conduction properties in scandia- and yttria-doped zirconia. The intrinsic differences of dopants are analyzed through the study of local charge densities. Furthermore, YSZ and ScSZ electrolytes are also synthesized and measured to verify the computational results.

II. COMPUTATIONAL AND EXPERIMENTAL METHODS

The calculations were performed within the framework of DFT as implemented in the Vienna *ab initio* simulation package (VASP) codes [18,19] with the generalized gradient approximation (GGA) for the exchange-correlation potential [20]. Projector-augmented-wave (PAW) pseudopotentials [21,22] are used to describe the interactions between ions and valence electrons. Valence-electron configurations are $5s^1 4d^3$ for Zr, $3s^2 3p^6 4s^2 3d^1$ for Sc, $4s^2 4p^6 5s^2 4d^1$ for Y, and $2s^2 2p^4$ for O [16]. The energy cutoff is chosen to be 500 eV for the plane wave basis. We employ a supercell containing 96 atomic sites for all bulk and defect structure calculations. $N_{Sc(Y)}/(N_{Sc(Y)} + N_{(Zr)})$ is defined as the doping concentration and dopants randomly occupy the Zr sites determined by the special quasirandom structure (SQS) method [23]. Density of states (DOS) are calculated with the Heyd-Scuseria-Ernzerhof- (HSE-) screened hybrid density functional to obtain accurate band-gap values. An $8 \times 8 \times 8$ Monkhorst-Pack grid is used for Brillouin-zone sampling [24]. The above parameters have also been employed in previous calculations [10,16,25–27]. The optimized lattice parameters are presented in Table I, which match well with the computational and experimental values.

TABLE I. Cubic, tetragonal, and monoclinic zirconia optimized lattice parameters. (Only nontrivial parameters are presented.)

Phase	This work	Expt. [28,29]	Other theory [30–32]
Cubic	$a = 5.1308$ Å	$a = 5.1308$ Å	$a = 5.1280$ Å
Tetragonal	$a = 5.1394$ Å	$a = 5.1274$ Å	$a = 5.1310$ Å
	$c = 5.2444$ Å	$c = 5.2143$ Å	$c = 5.2270$ Å
Monoclinic	$a = 5.2172$ Å	$a = 5.1503$ Å	$a = 5.1974$ Å
	$b = 5.2693$ Å	$b = 5.2018$ Å	$b = 5.2798$ Å
	$c = 5.3858$ Å	$c = 5.3146$ Å	$c = 5.3698$ Å
	$\beta = 99.92°$	$\beta = 99.26°$	$\beta = 99.53°$

ScSZ and YSZ powders are prepared using the coprecipitation method with NH_4OH (analytical-reagent grade, Xilong Chemical Co., Ltd., China), $ZrOCl_2$ (analytical-reagent grade, Tianyao Chemical Plant, Qingdao, China), Sc_2O_3 and Y_2O_3 (purity: 99.5%, Hunan General Research Institute of Nonferrous Metals, China), HCl (analytical-reagent grade, Xilong Chemical Co., Ltd., China). Precursors were calcined at 900 °C after filtering and washing with deionized water to remove the crystal water. Powders with particle size 0.5 μm are prepared by high-energy ball milling at 3000r for 15 min. Electrolytes are synthesized by dry pressing at 3000 lb and sintering at 1400 °C for 4 h. Methylcellulose and chloroplatinic acid are added to terpilenol for the Pt electrode slurry. The electrolyte conductivity is measured using the Direct Current 4-Probe Conductivity Testing Manual (Bloom Energy Co., Ltd, USA). Samples are tested several times at one temperature until the test values are consistent [33]. Diffusion barriers are calculated according to the Arrhenius plot [34]:

$$\ln \sigma T = -\frac{E}{kT} + \ln A, \qquad (1)$$

where k is Boltzmann's constant, $k = 0.86 \times 10^{-4}$, E is the diffusion barrier, T is the temperature (K), σ is conductivity, and A is the preexponential factor.

III. RESULTS AND DISCUSSIONS

A. Phase stability

Supercells with host cations, dopants, oxygen ions, and defects, as described in Sec. II, are built to calculate the total energy of specific configurations. In order to verify the accuracy of our calculations, E_{tot} of pure t and c phases were calculated. The energy difference between the two phases is 0.076 eV/unit, which is in agreement with the DFT GGA value of 0.062 eV/unit [30].

Figure 1 plots the total energy difference between the c and t phases of ScSZ and YSZ as a function of the doping concentration. The total energy of the t phase is set as zero for comparison. The total energy of the c phase is much
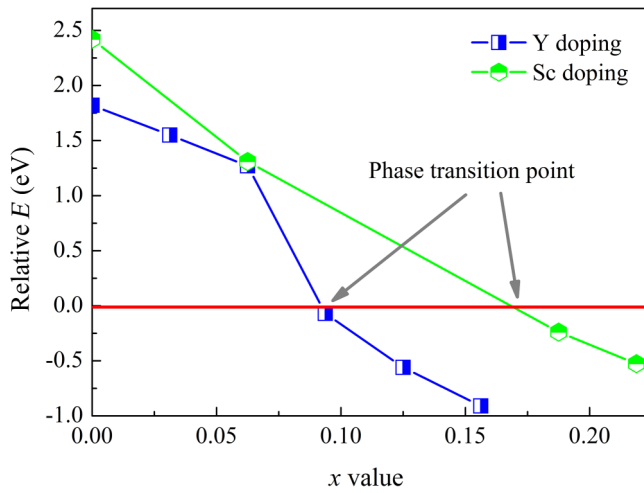
FIG. 1.   Calculated energy difference between c and t phases as a function of the doping concentration x for ScSZ and YSZ. The total energy of the tetragonal phase is set as zero.

higher than the t phase due to Zr atoms being too small to stabilize the c phase at room temperature. However, the energy difference decreases with an increase of doping concentration. The intersection of the curve and the zero line is the phase-transition doping concentration, which is 18 at. % for ScSZ. When the doping concentration is lower than 18 at. %, the t phase is more stable than the c phase. The c phase turns out to be more stable when the doping concentration is higher than 18 at. %. The phase-transition doping concentration of YSZ is 9 at. %. According to previous experimental results, the c phase can be stabilized at a doping concentration of 20 at. % for ScSZ [35,36] and 8 at. % for YSZ. These are in reasonable agreement with our calculated results.

The phase transition through doping is considered to be related to the geometric effects. The volume change caused by doping at various doping levels follows the same trend of the energy difference. This can be understood by the fact that Zr sites prefer to be sevenfold coordinated as in the m phase but not eight coordinated. After doping with Y^{3+} or Sc^{3+}, the atom packing becomes looser so that Zr atoms can adjust the local structure to reduce the total energy, which accompanies the increase of lattice volumes. As a result, proper dopants can stabilize the c phase by reducing the coordination number and increasing the local space for host cations [16].

B. Electronic structures

In order to study the intrinsic mechanism of phase transition, we perform electronic structure calculations for ScSZ and YSZ with different doping levels. The total density of states (TDOS) are plotted in Fig. 2. Because the multielectron interaction energy cannot be fully described by GGA, HSE is chosen to obtain more accurate valence-band-width and band-gap values [24,37]. The O s orbit contributes to

TABLE II.   ScSZ band-gap values of different doping concentrations.

Doping level (at. %)	Band-gap values (eV)
6.25	4.3930
18.75	4.2534
21.88	4.2310
25	4.2055

the DOS located at the low-energy region of around -20 eV, Zr d states and O p states combine to form the valence and conduction bands. The low-energy regions are aligned to compare the width of valence-band and band-gap values in Fig. 2. It is well known that the DOS peak will be a vertical line when the atoms are isolated, and when there is an interaction between the atoms, the density peak will be broadened [38]. On the other hand, the band-gap values also reveal the interactions and distance between the atoms. The interaction between atoms is strong if the atomic orbitals have a large overlap in the energy space [39]. According to these principles, the distance and interaction of atoms are determined by judging the width of the valence band in Fig. 2 and band-gap values in Tables II and III. The band-gap values are about 4.2 eV, which is higher than the 3.9 eV value calculated using the PHONOPY code and closer to the experimental value of 4.19 eV [40]. The valence-band-width and band-gap values of both ScSZ and YSZ decrease with an increase of doping amount. This indicates that with an increase of doping amount, the interaction between atoms becomes weaker, which is beneficial for stabilizing the higher energy cubic phase at room temperature. Therefore, the phase transition can be understood from lattice volume and local atomic structures.

C. Defect energies

In this section, the formation and binding energies of oxygen-vacancy and oxygen-defect complexes are investigated. $E_{\text{form}}(V_O)$ and $E_{\text{form}}(M\text{-}V_O\text{-}M)$ are defined as follows [41]:

$$E_{\text{form}}(V_O) = E_{Zr_{32-N}M_N O_{63}} - E_{Zr_{32-N}M_N O_{64}} + \mu_O, \quad (2)$$

$$E_{\text{form}}(M\text{-}V_O\text{-}M) = E_{Zr_{30}M_2 O_{63}} - E_{Zr_{32}O_{64}}$$
$$- 2\mu_M + 2\mu_{Zr} + \mu_O, \quad (3)$$

TABLE III.   YSZ band-gap values of different doping concentrations.

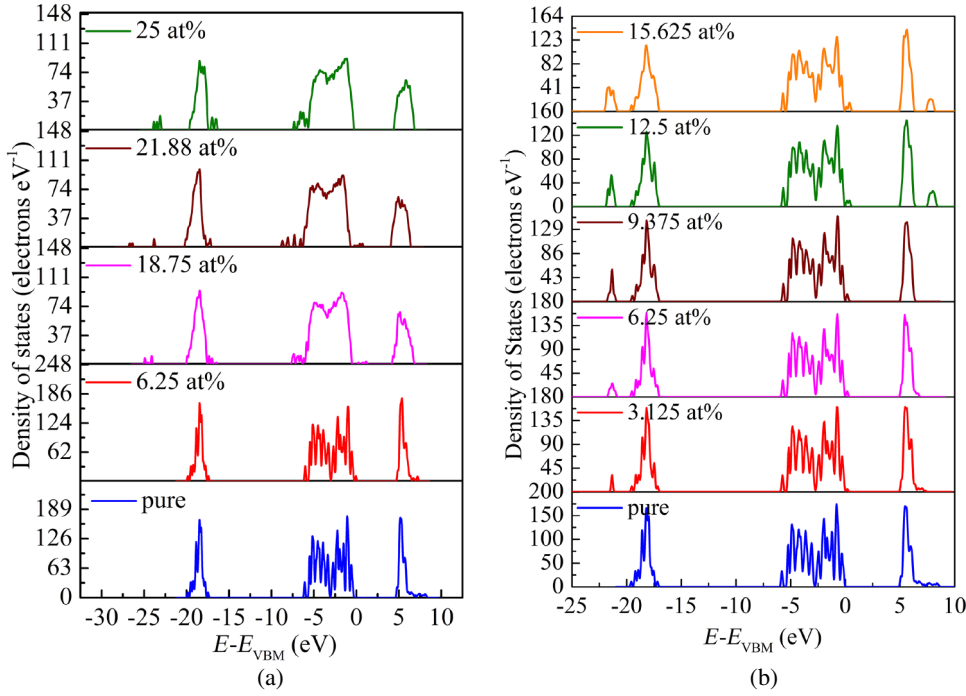| Doping level (at. %)	Band-gap values (eV)
3.125	4.1906
6.25	4.1760
9.375	4.0966
12.5	3.9994
15.625	3.8761

FIG. 2. (a) ScSZ and (b) YSZ total density of states of different doping concentrations.

where $E_{Zr_{32-N}M_NO_{63}}$ and $E_{Zr_{32-N}M_NO_{64}}$ are the total energies of zirconia doped with M, $E_{Zr_{32}O_{64}}$ is the total energy of pure structure, μ_i ($i = $ M, Zr, O) is the chemical potential of atom i.

If we apply

$$\mu_{Zr} + 2\mu_O = \mu_{ZrO_2} \tag{4}$$

$$2\mu_M + 3\mu_O = \mu_{M_2O_3}, \tag{5}$$

then we have

$$E_{form}(M\text{-}V_O\text{-}M) = E_{Zr_{30}M_2O_{63}} - E_{Zr_{32}O_{64}}$$
$$- \mu_{M_2O_3} + 2\mu_{ZrO_2}, \tag{6}$$

where $\mu_{M_2O_3}$ and μ_{ZrO_2} are the total energies of M_2O_3 and ZrO_2 in the bulk phase, respectively. The formation energies of the atomic configurations shown in Fig. 3 are calculated.

Table IV lists the oxygen-vacancy-formation energies of undoped and doped ZrO_2. The oxygen-vacancy-formation energy is 5.53 eV (undoped) under oxygen-rich conditions. Previous theoretical results reported that the formation energy of neutral V_O of undoped ZrO_2 is 6.11 eV [42]. Zheng *et al.* reported [37] that the V_O formation energy in zirconia is 6.26 eV. Furthermore, Eichler reported a formation energy of 5.73 eV calculated by the GGA [43]. Our calculated results show that it is easier to form oxygen vacancies in the doped ZrO_2 compared with the undoped case.

Researchers are still debating which cation the oxygen vacancy prefers to bind with. V_O and dopants have a charge of $+2$ and -1, and they attract each other

from an electrostatic point of view. However, the elastic interactions may lead to a repulsion interaction between dopants and V_O. M-V_O-M-complex-formation energies are calculated according to formula (6) and the results are plotted in Fig. 4. According to our calculations, E_{form} of Y-V_O-Y is 8.39 and 8.96 eV for the 2NN and 1NN configurations, respectively. This indicates that V_O at the 2NN site is easier to form than at the 1NN site. But for Sc-V_O-Sc, E_{form} is almost the same for the 1NN and 2NN sites, which indicates that V_O does not prefer to form at a specific site. This phenomenon is helpful for oxygen vacancies to diffuse among various sites in ScSZ. It may explain why ScSZ exhibits a relatively higher conductivity than YSZ [33,34,44].

In order to further verify the results that the 2NN-site V_O is easier to form in YSZ, we calculate the total energies with V_O located at various sites (Fig. 5). The total energy results are shown in Fig. 6. The lowest-energy point appears at the 2NN site, while the 1NN site has the highest energy. Differing from the opinion that Y_{Zr} and V_O are arranged at the 1NN positions [45], our results indicate that V_O prefers to stay at the 2NN sites of Y_{Zr}. The

TABLE IV. Oxygen-vacancy-formation energies of undoped and doped ZrO_2. All units are in eV. $\mu_0 \leq -4.92$ eV.

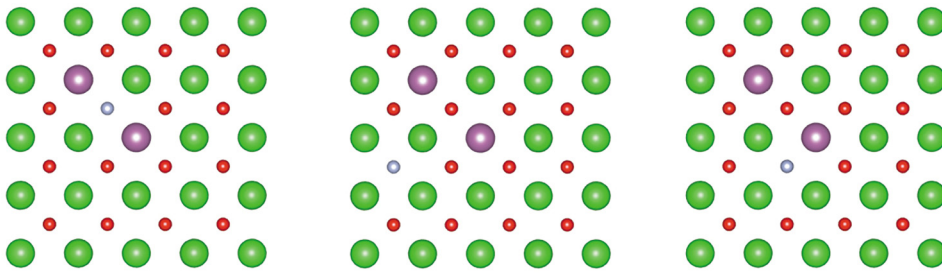|	E_f (undoped)	E_f (doping M/Zr = 1/32)	E_f (doping M/Zr = 2/32)
Y	$10.45 + \mu_0$	$7.74 + \mu_0$	$3.96 + \mu_0$
Sc		$7.61 + \mu_0$	$4.16 + \mu_0$

FIG. 3. Defect configurations of zirconia doped with Y or Sc. (From left to right: nearest neighbor [1NN], next-nearest neighbor [2NN], 1NN to one doping atom and 2NN to another one. Purple balls, doping atoms Y or Sc; green balls, Zr atom; red balls, O atom; gray balls, V_O.)

oxygen vacancy and dopant locations are also investigated by some x-ray, electron, and neutron diffractions [46–48].

The above results can be explained by elastic interactions. The ion radii of Zr (eightfold coordinated), Sc (six coordinated), and Y (six coordinated) are 72, 74, and 90 pm. V_O prefers to locate at a specific site, which reduces the lattice distortion caused by Y doping. While for Sc doping, V_O does not need to occupy a specific site to reduce the distortion effect due to the similar radii of Sc^{3+} and Zr^{4+}.

However, not all oxygen vacancies can freely diffuse because single negatively charged defect M_{Zr} would bind with V_O due to the electrostatic interaction. Filal also pointed out that the conductivity of YSZ is controlled by the associated point defects (Y_{Zr}-V_O) [49]. The binding energies are calculated in this section to determine the interaction between the M_{Zr} defect and oxygen vacancy. It is defined as follows:

$$\Delta E_{bind} = \Delta E_{form}(V_O) + \Delta E_{form}(M_{Zr}) \\ - \Delta E_{form}(V_O + M_{Zr}), \quad (8)$$

where ΔE_{form} is the formation energy of each defect. Figure 7 shows that the E_{bind} value is 0.2–0.4 eV for Sc-V_O and 0.5–0.8 eV for Y-V_O. Zacate et al. reported a binding-energy value of 0.2 eV for Sc-V_O, 0.4 eV for Y-V_O, 0.4 eV for Sc-V_O-Sc and 0.6 eV for Y-V_O-Y by a Born-like model [50]. Eichler reported a binding energy of 0.1–0.5 eV as a function of the Y-Vo distance [43]. In addition, the binding energies reported by other papers [51,52] are almost in the same range.

The binding-energy differences between the two defect configurations are 0.01 and 0.26 eV for Sc-V_O-Sc and Y-V_O-Y, respectively. This indicates that little energy is needed for V_O to diffuse from the 1NN site to the 2NN site and escape from the Sc^{3+} ion. Conversely, there is a significant difference between the binding energies of the 1NN and 2NN configurations in YSZ. As discussed above, for YSZ, the elastic repulsion results in a structural distortion and strong defect interaction that hinders the diffusion of oxygen vacancies [13,53].

D. Differential charge density

Differential charge densities are defined as follows:

$$\Delta \rho = \rho(Zr_{32-y}M_yO_{64-x}) - \rho(Zr_{32}O_{64}) \\ - y\rho(M) + y\rho(Zr) + x\rho(O). \quad (9)$$

In Fig. 8(a), the yellow areas represent electron gaining, and the blue areas indicate electron depletion. Y^{3+} only influences the charge density of 1NN oxygen atoms in YSZ. Y atoms transfer their electrons to O atoms and form the Y−O chemical bonds. In the Y-doped case, there is no
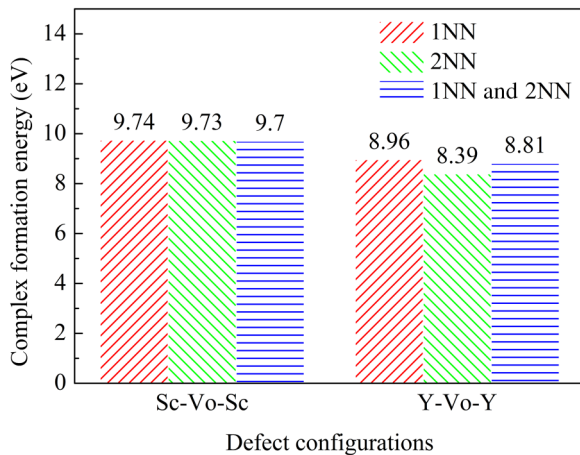

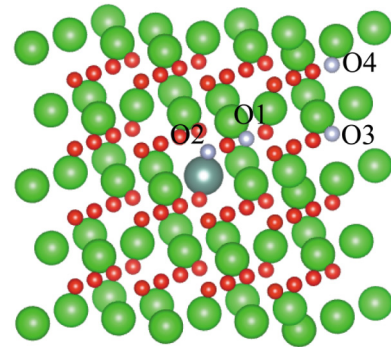FIG. 4. Different configuration formation energies. E_{form} is almost the same for the 1NN and 2NN sites of ScSZ.

FIG. 5. Y-V_O configurations of different distances. (Green balls, Zr atom; red balls, O atom; blue ball, Y atom; gray balls, V_O.)
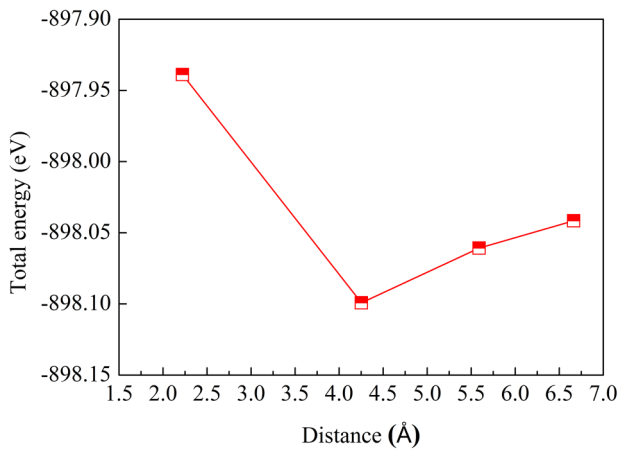
FIG. 6. Total energy vs. Y-V_O distance. (From left to right: 1NN, 2NN, 3NN, 4NN.) The lowest energy point appears at the 2NN site.

charge-density change for the 2NN oxygen atoms. When doped with Sc^{3+} [Fig. 8(b)], both the 1NN- and 2NN-site oxygen atoms show charge transfer, which indicates that the electrons of those oxygen atoms are influenced by Sc^{3+}. This phenomenon is also found in the doped *t* zirconia shown in Figs. 8(c) and 8(d). It is speculated that the charge transfer of oxygen may be beneficial for oxygen diffusion to the interstitial sites. Both 1NN- and 2NN-site oxygen ions are able to diffuse in ScSZ. The Polaris ability of Sc^{3+} may be responsible for this result. Conversely, only 1NN-site oxygen ions are able to diffuse in YSZ. The complex formation and binding energies in the above section may be correlated to the local charge densities. We argue that the local charge-density change is the intrinsic influence of dopants on ionic conduction properties in zirconia.
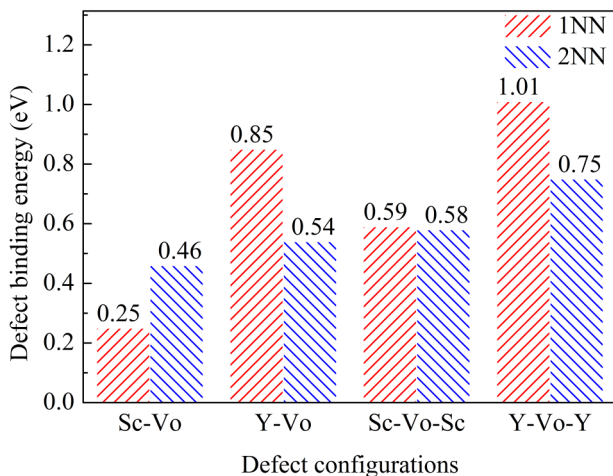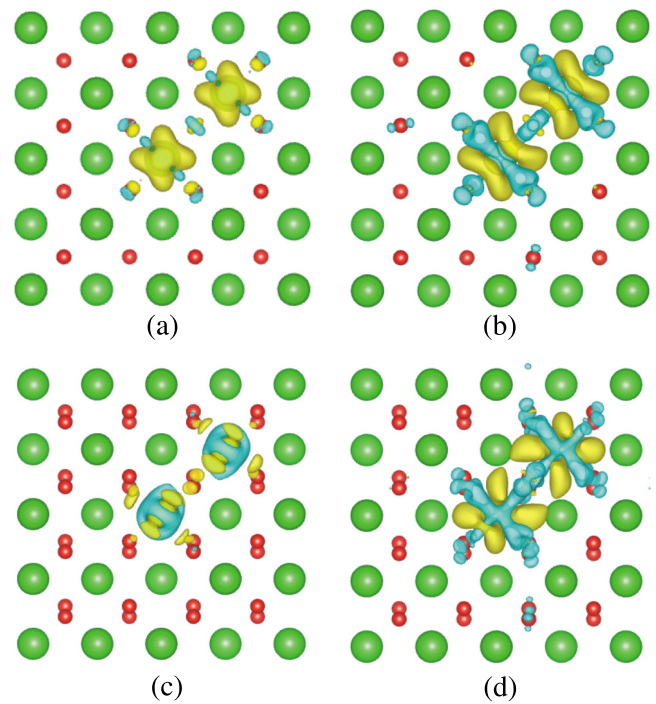

FIG. 8. Differential charge densities of *c* and *t* phase doped with Y and Sc [(a) *c* phase, doped *Y*; (b) *c* phase, doped Sc; (c) *t* phase, doped Y; (d) *t* phase, doped Sc].

E. Oxygen diffusion barriers

The saddle-point method is employed to study the diffusion barriers of oxygen atoms in ScSZ and YSZ. The saddle point is assumed to be located at the plane that has the following properties: it is perpendicular to the shortest path and contains the other two cations [54]. The diffusion barrier is the energy difference between the saddle-point energy and the initial state energy. In this section, diffusion barriers of ⟨100⟩, ⟨101⟩, and ⟨111⟩ directions, as shown in Fig. 9, are calculated.

The diffusion barrier of ScSZ is smaller than YSZ for all three diffusion directions (see Table V). Diffusion barriers
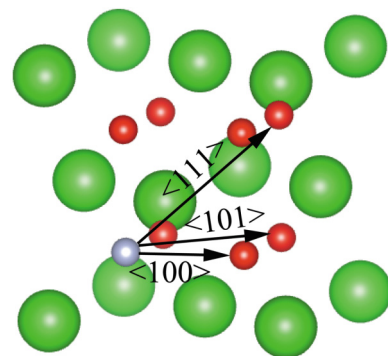

FIG. 7. Defect complex binding energies. Binding energy of defect complexes in ScSZ is lower than in YSZ.

FIG. 9. Schematic diagram of ⟨100⟩, ⟨101⟩, and ⟨111⟩ directions in zirconia.

TABLE V.   Diffusion barriers of different directions in YSZ and ScSZ.

Configurations	Diffusion barriers (eV)	
	YSZ	ScSZ
$\langle 100 \rangle$ direction	0.91	0.80
$\langle 101 \rangle$ direction	1.12	0.92
$\langle 111 \rangle$ direction	1.59	1.14

of the $\langle 100 \rangle$ direction is the smallest among all three directions. Similar results were also reported in other literature [55]. This indicates that oxygen atoms prefer to diffuse through the $\langle 100 \rangle$ direction. The obtained diffusion barriers are also verified by experiments. Ionic conductivities of different temperatures are measured by the direct current four-probe method. The slope of $\ln \sigma T$-$1/T$, as shown in Fig. 10, represents the diffusion barrier according to the Arrhenius formula. The experimental diffusion barrier of YSZ and ScSZ is 0.92 and 0.83 eV, respectively. Other researchers' results are also in the range of 0.8–1.2 and 0.7–0.9 eV [56,57]. Badwal reported that ionic conductivity of YSZ is lower than that in ScSZ for all measured temperature ranges [58], which is in agreement with our theoretical and experimental results.
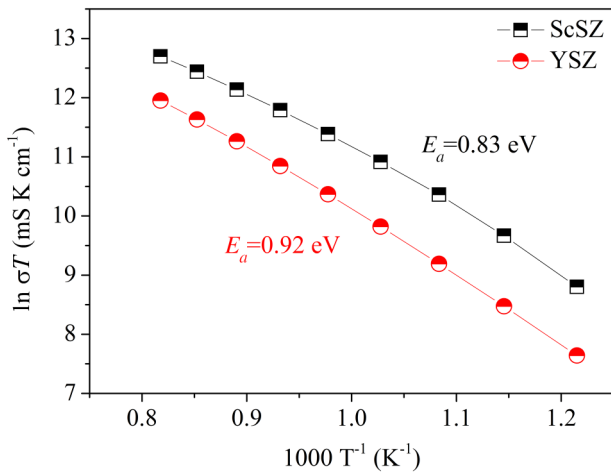

FIG. 10.   Arrhenius plots of YSZ and ScSZ electrolytes.

IV. CONCLUSIONS

In this paper, the phase stability and defect interaction in doped zirconia are investigated using DFT calculations and experiments. The doping concentrations of the tetragonal-to-cubic phase transition are predicted to be 18 at. % for Sc^{3+} and 9 at. % for Y^{3+}. The atom packing becomes looser and Zr atoms adjust the local structure to reduce the total energy upon yttria and scandia doping. Oxygen-vacancy-formation energies, oxygen-vacancy-dopant binding energies, and diffusion barriers are

calculated to evaluate ionic conduction properties of cubic zirconia. Results show that formation-energy and binding-energy differences of different structural configurations in scandia-doped zirconia are lower than those in yttria-doped zirconia, which is beneficial for oxygen vacancies to diffuse through the zirconia lattice. The differential charge-density calculations show that both the 1NN- and 2NN-site oxygen atoms show charge transferring for the scandia-doping case, but charge transferring occurs only at the 1NN-site oxygen atoms when it is doped with yttria. Diffusion barriers are calculated using the saddle-point method, and the corresponding experiments are carried out to verify the diffusion-barrier results.

[1] T. H. Shin, M. Shin, G. W. Park, S. Lee, S. K. Woo, and J. Yu, Fabrication and characterization of oxide ion conducting films, $Zr_{1-x}M_xO_{2-\delta}$ (M = Y, Sc) on porous SOFC anodes, prepared by electron beam physical vapor deposition, Sust. Energ. Fuels **1,** 103 (2017).

[2] N. M. Farandos, L. Kleiminger, T. Li, A. Hankin, and G. H. Kelsall, Three-dimensional inkjet printed solid oxide electrochemical reactors. I. Yttria-stabilized zirconia electrolyte, Electrochim. Acta **213,** 324 (2016).

[3] H. J. Kim, M. Kim, C. N. Ke, G. D. Han, K. Bae, J. M. Shin, G. T. Kim, and J. H. Shim, Slurry spin coating of thin film yttria stabilized zirconia/gadolinia doped ceria bi-layer electrolytes for solid oxide fuel cells, J. Power Sources **327,** 401 (2016).

[4] A. Kuwabara, T. Tohei, T. Yamamoto, and I. Tanaka, Ab initio lattice dynamics and phase transformations of ZrO_2, Phys. Rev. B **71,** 064301 (2005).

[5] N. Mahato, A. Banerjee, A. Gupta, S. Omar, and K. Balani, Progress in material selection for solid oxide fuel cell technology: A review, Prog. Mater. Sci. **72,** 141 (2015).

[6] S. Vasanthavel, B. Derby, and S. Kannan, Tetragonal to cubic transformation of SiO_2-stabilized ZrO_2 polymorph through dysprosium substitutions, Inorg. Chem. **56,** 1273 (2017).

[7] M. A. Taylor, M. Kilo, G. Borchardt, S. Weber, and H. Scherrer, 96 Zr diffusion in polycrystalline scandia stabilized zirconia, J. Eur. Ceram. Soc. **25,** 1591 (2005).

[8] T. H. Etsell and S. N. Flengas, Electrical properties of solid oxide electrolytes, Chem. Rev. **70,** 339 (1970).

[9] V. Venkatesh and C. V. Reddy, Thermal and electrical properties of $Ce_{0.8-x}Pr_xSm_{0.2}O_{2-\delta}$ electrolyte materials for IT-SOFC applications, Ionics **23,** 3455 (2017).

[10] D. Marrocchelli, P. A. Madden, S. T. Norberg, and S. Hull, Structural disorder in doped zirconias, Part II: Vacancy ordering effects and the conductivity maximum, Chem. Mater. **23,** 1365 (2015).

[11] A. M. Iskandarov, Y. Ding, and Y. Umeno, Effect of cation dopants in zirconia on interfacial properties in nickel/zirconia systems: An atomistic modeling study, J. Phys. Condens. Matter **29**, 045001 (2016).

[12] M. Raza, D. Cornil, J. Cornil, S. Lucas, R. Snyders, and S. Konstantinidis, Oxygen vacancy stabilized zirconia (OVSZ); a joint experimental and theoretical study, Scr. Mater. **124**, 26 (2016).

[13] A. R. Puigdollers, F. Illas, and G. Pacchioni, Structure and properties of zirconia nanoparticles from density functional theory calculations, J. Phys. Chem. C **120**, 4392 (2016).

[14] S. P. Miller, B. I. Dunlap, and A. S. Fleischer, Cation coordination and interstitial oxygen occupancy in co-doped zirconia from first principles, Solid State Ionics **227**, 66 (2012).

[15] Y. Zhang and J. Zhang, First principles study of structural and thermodynamic properties of zirconia, Mater. Today Proc. **1**, 44 (2014).

[16] Q. Xue, X. Huang, L. Wang, J. Dong, H. Xu, and J. Zhang, Effects of Sc doping on phase stability of $Zr_{1-x}Sc_xO_2$ and phase transition mechanism: First-principles calculations and Rietveld refinement, Mater. Des. **114**, 297 (2017).

[17] R. J. Stafford, S. J. Rothman, and J. L. Routbort, Effect of dopant size on the ionic conductivity of cubic stabilised ZrO_2, Solid State Ionics **37**, 67 (1989).

[18] G. Kresse and J. Hafner, Ab initio molecular dynamics for liquid metals, Phys. Rev. B Condens. Matter **47**, 558 (1993).

[19] G. Kresse and J. Furthmüller, Efficient iterative schemes for ab initio total-energy calculations using a plane-wave basis set, Phys. Rev. B Condens. Matter **54**, 11169 (1996).

[20] J. P. Perdew, K. Burke, and M. Ernzerhof, ERRATA: Generalized Gradient Approximation made Simple, Phys. Rev. Lett. **77**, 3865 (1996).

[21] P. E. Blöchl, Projector agmented-wave method, Phys. Rev. B **50**, 17953 (1994).

[22] G. Kresse and D. Joubert, From ultrasoft pseudopotentials to the projector augmented-wave method, Phys. Rev. B **59**, 1758 (1999).

[23] L. G. Wang, Y. Xiong, W. Xiao, L. Cheng, J. Du, H. Tu, and A. van de Walle, Computational investigation of the phase stability and the electronic properties for Gd-doped HfO_2, Appl. Phys. Lett. **104**, 247 (2014).

[24] J. Heyd and G. E. Scuseria, Efficient hybrid density functional calculations in solids: Assessment of the Heyd–Scuseria–Ernzerhof screened Coulomb hybrid functional, J. Chem. Phys. **121**, 1187 (2004).

[25] N. Wei, X. Zhang, C. Zhang, S. Hou, and Z. Zeng, First-principles investigations on the elastic and thermodynamic properties of cubic ZrO_2 under high pressure, Int. J. Mod. Phys. C **26**, 1897 (2015).

[26] J. Cizek, O. Melikhova, I. Procházka, J. Kuriplach, R. Kužel, G. Brauer, W. Anwand, T. E. Konstantinova, and I. A. Danilenko, Defect studies of nanocrystalline zirconia powders and sintered ceramics, Phys. Rev. B Condens. Matter **81**, 1718 (2010).

[27] X. Y. Zhao and D. Vanderbilt, Phonons and lattice dielectric properties of zirconia, Phys. Rev. B **65**, 7 (2001).

[28] H. A. Abbas, F. F. Hamad, A. K. Mohamad, Z. M. Hanafi, and M. Kilo, Structural properties of zirconia doped with some oxides, Diff. Fund. **8**, 7.1 (2013).

[29] K. A. Khor and J. Yang, Lattice parameters, tetragonality (c/a) and transformability of tetragonal zirconia phase in plasma-sprayed ZrO_2 -Er_2O_3 coatings, Mater. Lett. **31**, 23 (1997).

[30] J. E. Jaffe, R. A. Bachorz, and M. Gutowski, Low-temperature polymorphs of ZrO_2 and HfO_2: A density-functional theory study, Phys. Rev. B **72**, 144107 (2005).

[31] G. Fadda, L. Colombo, and G. Zanzotto, First-principles study of the structural and elastic properties of zirconia, Phys. Rev. B Condens. Matter **79**, 1377 (2009).

[32] G. Jomard, T. Petit, A. Pasturel, L. Magaud, G. Kresse, and J. Hafner, First principles calculations to describe zirconia pseudopolymorphs, MRS Proc. **492**, 4044 (1997).

[33] P. M. Abdala, G. S. Custo, and D. G. Lamas, Enhanced ionic transport in fine-grained scandia-stabilized zirconia ceramics, J. Power Sources **195**, 3402 (2010).

[34] S. Sarat, N. Sammes, and A. Smirnova, Bismuth oxide doped scandia-stabilized zirconia electrolyte for the intermediate temperature solid oxide fuel cells, J. Power Sources **160**, 892 (2006).

[35] E. Courtin, P. Boy, C. Rouhet, L. Bianchi, E. Bruneton, N. Poirot, C. Labertyrobert, and C. Sanchez, Optimized sol–gel routes to synthesize yttria-stabilized zirconia thin films as solid electrolytes for solid oxide fuel cells, Chem. Mater. **24**, 4540 (2012).

[36] G. Suárez and Y. Sakka, Effect of alumina addition on initial sintering of cubic ZrO_2 (8YSZ), Ceram. Int. **36**, 879 (2010).

[37] J. X. Zheng, G. Ceder, T. Maxisch, W. K. Chim, and W. K. Choi, First-principles study of native point defects in hafnia and zirconia, Phys. Rev. B Condens. Matter **75**, 104112-1 (2007).

[38] A. Luff, Role of oxygen vacancies on the structure and density of states of iron-doped zirconia, Phys. Rev. B Condens. Matter **87**, 178 (2012).

[39] I. I. Mazin and V. I. Anisimov, Insulating gap in FeO: Correlations and covalency, Phys. Rev. B **55**, 12822 (1996).

[40] M. Youssef and B. Yildiz, Intrinsic point-defect equilibria in tetragonal ZrO_2: Density functional theory analysis with finite-temperature effects, Phys. Rev. B **86**, 8043 (2012).

[41] L. G. Wang, H. L. Tu, Y. H. Xiong, and W. Xiao, Formation of the dopant-oxygen vacancy complexes and its influence on the photoluminescence emissions in Gd-doped HfO_2, J. Appl. Phys. **116**, 7399 (2014).

[42] H. Zhang, B. Gao, B. Sun, G. Chen, L. Zeng, L. Liu, X. Liu, J. Lu, R. Han, and J. Kang, Ionic doping effect in ZrO_2 resistive switching memory, Appl. Phys. Lett. **96**, 093509 (2010).

[43] A. Eichler, Tetragonal Y-doped zirconia: Structure and ion conductivity, Phys. Rev. B **64**, 607 (2001).

[44] A. A. Jais, S. A. M. Ali, M. Anwar, M. R. Somalu, A. Muchtar, N. R. W. I. Wan, C. Y. Tan, R. Singh, and N. P. Brandon, Enhanced ionic conductivity of scandia-ceria-stabilized-zirconia (10Sc1CeSZ) electrolyte synthesized by

the microwave-assisted glycine nitrate process, Ceram. Int. **43**, 8119 (2017).

[45] M. Weller and H. Schubert, Internal friction, dielectric loss, and ionic conductivity of tetragonal ZrO_2-3% Y_2O_3 (Y-TZP), J. Am. Ceram. Soc. **69**, 573 (1986).

[46] J. P. Goff, W. Hayes, S. Hull, M. T. Hutchings, and K. N. Clausen, Defect structure of yttria-stabilized zirconia and its influence on the ionic conductivity at elevated temperatures, Phys. Rev. B **59**, 14202 (1999).

[47] S. García-Martín, M. A. Alario-Franco, D. P. Fagg, and J. T. S. Irvine, Evidence of three types of short range ordered fluorite structure in the (1-x) $Y_{0.15}Zr_{0.85}O_{1.93} - x$ $Y_{0.75}Nb_{0.25}O_{1.75}$ $(0 \leq x \leq 1)$ system, J. Mater. Chem. **15**, 1903 (2005).

[48] S. Garcia-Martin, M. A. Alario-Franco, D. P. Fagg, A. J. Feighery, and J. T. S. Irvine, Modulated fluorite-type structure of materials from the (1-x)$Y_{0.5}Zr_{0.5}O_{1.75}$-$xY_{0.75}Nb_{0.25}O_{1.75}$ $(0 \leq x \leq 1)$ system, Mater. Chem. **12**, 1729 (2000).

[49] M. Filal, C. Petot, M. Mokchah, C. Chateau, and J. L. Carpentier, Ionic conductivity of yttrium-doped zirconia and the "composite effect", Solid State Ionics **80**, 27 (1995).

[50] M. O. Zacate, L. Minervini, D. J. Bradfield, R. W. Grimes, and K. E. Sickafus, Defect cluster formation in M_2O_3 -doped cubic ZrO_2, Solid State Ionics **128**, 243 (2000).

[51] M. S. Khan, M. S. Islam, and D. R. Bates, Cation doping and oxygen diffusion in zirconia: A combined atomistic simulation and molecular dynamics study, J. Mater. Chem. **8**, 2299 (1998).

[52] Y. Arachi, H. Sakai, O. Yamamoto, Y. Takeda, and N. Imanishai, Electrical conductivity of the ZrO_2 –Ln_2O_3 (Ln = lanthanides) system, Solid State Ionics **121**, 133 (1999).

[53] H. Ding, A. V. Virkar, and F. Liu, Defect configuration and phase stability of cubic versus tetragonal yttria-stabilized zirconia, Solid State Ionics **215**, 16 (2012).

[54] R. Pornprasertsuk, P. Ramanarayanan, C. B. Musgrave, and F. B. Prinz, Predicting ionic conductivity of solid oxide fuel cell electrolyte from first principles, J. Appl. Phys. **98**, 4106 (2005).

[55] J. A. Hirschfeld, and H. Lustfeld, First-principles study and modeling of strain-dependent ionic migration in ZrO_2, Phys. Rev. B **84**, 2461 (2011).

[56] V. V. Lakshmi, R. Bauri, A. S. Gandhi, and S. Paul, Synthesis and characterization of nanocrystalline ScSZ electrolyte for SOFCs, Int. J. Hydrogen Energy **36**, 14936 (2011).

[57] K. J. Albrecht and R. J. Braun, The effect of coupled mass transport and internal reforming on modeling of solid oxide fuel cells part I: Channel-level model development and steady-state comparison, J. Power Sources **304**, 384 (2016).

[58] S. P. S. Badwal, Zirconia-based solid electrolytes: Microstructure, stability and ionic conductivity, Solid State Ionics **52**, 23 (1992).